AD-A252 076

|||||||||||||||||||||||

S DTIC
ELECTE
JUN 16 1992
A D

Effects of Inhomogeneous Filtering and Buoyant Forcing on the Dynamic Subgrid Scale Model

M. Bohnert

J. H. Ferziger

Center for Large Scale Scientific Computation
Building 460, Room 313
Stanford University
Stanford, California 94305

92-15387

||||||||||||||||||||||

92 6 12 047

REPORT DOCUMENTATION PAGE

Form Approved
OMB No. 0704-0188

1a. REPORT SECURITY CLASSIFICATION UNCLASSIFIED	1b. RESTRICTIVE MARKINGS NONE
2a. SECURITY CLASSIFICATION AUTHORITY	3. DISTRIBUTION/AVAILABILITY OF REPORT
2b. DECLASSIFICATION/DOWNGRADING SCHEDULE	Unlimited

4. PERFORMING ORGANIZATION REPORT NUMBER(S)

CLaSSiC Manuscript 92-30

5. MONITORING ORGANIZATION REPORT NUMBER(S)

6a. NAME OF PERFORMING ORGANIZATION Stanford University	6b. OFFICE SYMBOL (If applicable) 2E254	7a. NAME OF MONITORING ORGANIZATION Department of the Navy Office of Naval Research

6c. ADDRESS (City, State, and ZIP Code)
c/o Sponsored Projects Office
Encina Hall, 660 Arguello Way
Stanford, CA 94305

7b. ADDRESS (City, State, and ZIP Code)

800 North Quincy Street
Arlington, VA 22217-5000

8a. NAME OF FUNDING/SPONSORING ORGANIZATION Office of Naval Research	8b. OFFICE SYMBOL (If applicable) N00014	9. PROCUREMENT INSTRUMENT IDENTIFICATION NUMBER N00014-90-J-1344

8c. ADDRESS (City, State, and ZIP Code)

800 North Quincy Street
Arlington, VA 22217-5000

10 SOURCE OF FUNDING NUMBERS

PROGRAM ELEMENT NO.	PROJECT NO.	TASK NO	WORK UNIT ACCESSION NO

11. TITLE (Include Security Classification)
Effects of Inhomogeneous Filtering and Buoyant Forcing on the Dynamic Subgrid Scale Model

12. PERSONAL AUTHOR(S)
M. Bohnert and Joel Ferziger

13a. TYPE OF REPORT INTERIM	13b TIME COVERED FROM 90Jul TO 91Dec	14. DATE OF REPORT (Year, Month, Day) 92Feb	15 PAGE COUNT 30

16 SUPPLEMENTARY NOTATION

17 COSATI CODES			18. SUBJECT TERMS (Continue on reverse if necessary and identify by block number)
FIELD	GROUP	SUB-GROUP	

19 ABSTRACT (Continue on reverse if necessary and identify by block number)

The dynamic subgrid scale model is used in large-eddy simulation of the stratified Ekman layer. Results from direct numerical simulations (DNS) for the neutral Ekman layer were used to test model efficacy. Three dimensional test filtering was employed in the dynamic calculation. A significant increase in accuracy was observed in the neutral layer when this filtering was employed, as compared to filtering only in planes parallel to the surface. The model shows the ability to model both unstable and stable regions, and its effect vanishes where stratification strongly quenches the turbulence.

20. DISTRIBUTION/AVAILABILITY OF ABSTRACT ☒ UNCLASSIFIED/UNLIMITED ☐ SAME AS RPT ☐ DTIC USERS	21 ABSTRACT SECURITY CLASSIFICATION UNCLASSIFIED
22a. NAME OF RESPONSIBLE INDIVIDUAL Joel Ferziger	22b TELEPHONE (Include Area Code) (415) 723-3615 22c. OFFICE SYMBOL

DD Form 1473, JUN 86

Previous editions are obsolete.

SECURITY CLASSIFICATION OF THIS PAGE

S/N 0102-LF-014-6603

UNCLASSIFIED

Effects of Inhomogeneous Filtering and Buoyant Forcing

on the Dynamic Subgrid Scale Model

M. Bohnert and J. H. Ferziger

Dept. of Mech. Eng., Thermosciences Division

Stanford University, Stanford, California

Abstract

The dynamic subgrid scale model is used in large-eddy simulation of the stratified Ekman layer. Results from direct numerical simulations (DNS) for the neutral Ekman layer were used to test model efficacy. Three dimensional test filtering was employed in the dynamic calculation. A significant increase in accuracy was observed in the neutral layer when this filtering was employed, as compared to filtering only in planes parallel to the surface. The model shows the ability to model both unstable and stable regions, and its effect vanishes where stratification strongly quenches the turbulence.

Introduction

In large-eddy simulations of turbulence (LES), the largest scales are directly computed while the subgrid scales (SGS) are modelled. The latter are the scales that cannot be resolved. The majority of SGS modelling closures make use of eddy-viscosity parameterizations; the most popular is due to Smagorinsky[1] in which the eddy viscosity is represented as

$$\nu_T = (C_s \overline{\Delta})^2 |\overline{S}| \tag{1}$$

where $\overline{\Delta}$ is the filter length scale, C_s is a specified constant, and $|\overline{S}| = (2\overline{S}_{ij}\overline{S}_{ij})^{1/2}$ is the magnitude of the resolved strain rate tensor,

$$\overline{S}_{ij} = \frac{1}{2}(\frac{\partial \overline{u}_i}{\partial x_j} + \frac{\partial \overline{u}_j}{\partial x_i}) \tag{2}$$

While the Smagorinsky model has enjoyed success, its application to a wide variety of flows has been limited by the following factors:

(a) The viscosity does not vanish in laminar flow,

(b) The model is absolutely dissipative; that is, backscatter from small to large scales cannot be represented,

(c) *Ad hoc* modifications are often required in regions of large gradients (e.g. near a boundary),

(d) There is widespread debate among researchers about the value of C_s, with an apparent lack of a 'universal' value that can be used for a wide range of flows.

In addition to the above limitations present in engineering flows, the meteorological community has found that the Smagorinsky model is poorly suited to flows affected by unstable and stable stratification. The SGS parameterization in these flows commonly takes one of two forms[2]:

(e) Modifications to the basic Smagorinsky concept are employed; for example, C_s becomes a function of the local Richardson number,

(f) The eddy viscosity is determined by the local value of the SGS turbulent kinetic energy, e_S. This requires a solution of an additional equation for the transport of e_S.

<center>2</center>

Recently Germano *et al.*[3] proposed a dynamic subgrid scale model which calculates the Smagorinsky coefficient C_s interactively as a function of both space and time. The coefficient is computed *via* the application of a test filter with length scale $\overline{\overline{\Delta}} > \overline{\Delta}$ to the LES field. The resolved information contained between these two length scales is used to calculate C_s.

The dynamic model has been successful in both incompressible and compressible homogeneous flows, as well as incompressible turbulent and transitional channel flows[3,4]. None of the limitations (a)-(c) listed above are evident (limitation (d) is no longer meaningful since C_s is not constant). In turbulent channel flow, however, the test filter has only been applied in two dimensions; these are the planes parallel to the walls on which the computational grid is uniform.

The purpose of this study is to investigate the applicability of the dynamic SGS model in the LES of a stratified external wall-bounded flow, the turbulent Ekman layer. The efficacy of three-dimensional test filtering, including an inhomogeneous direction in which the grid is not uniform, is examined and compared to the previously used two-dimensional approach. A temperature profile with unstable and stable regions will be imposed on the flow to introduce buoyantly-forced turbulent dynamics. This stratified flow is an idealization of a meterological application, the Convective Boundary Layer (CBL), and will be used to examine the applicability of the dynamic model in flows where parameterizations (e) and (h) above had previously been employed.

Problem Formulation and Numerical Method

We consider the flow of a stratified viscous fluid, driven by a uniform pressure gradient (geostrophic conditions aloft) and experiencing steady system rotation. Density variations are assumed to have no dynamic influence other than to provide a temperature dependent body force (the 'Boussinesq' approximation). A three dimensional filter that commutes with differentiation is applied to the governing equations; filtering the nonlinear terms results in a subgrid scale stress and heat flux, τ_S and q_s, respectively :

$$\frac{\partial \overline{u}_i}{\partial t} + \frac{\partial}{\partial x_j}(\overline{u}_i\overline{u}_j) = -\frac{1}{\rho_\infty}\frac{\partial \overline{p}}{\partial x_i} + 2\epsilon_{ijk}\Omega_j(G_k - \overline{u}_k) + \delta_{i3}(\overline{\theta} - <\overline{\theta}>)g + \nu\frac{\partial^2 \overline{u}_i}{\partial x_j \partial x_j} - \frac{\partial \tau_{S,ij}}{\partial x_j} \quad (3)$$

$$\frac{\partial \bar{u}_j}{\partial x_j} = 0 \tag{4}$$

$$\frac{\partial \bar{\theta}}{\partial t} + \frac{\partial}{\partial x_j}(\bar{u}_j \bar{\theta}) = \kappa \frac{\partial^2 \bar{\theta}}{\partial x_j \partial x_j} - \frac{\partial q_{S,j}}{\partial x_j} \tag{5}$$

Here, Ω_i is the applied rotation and G_i is the free stream velocity, which along with the acceleration of gravity, g, define the imposed uniform pressure gradient

$$\frac{\partial \bar{P}}{\partial x_i} = -2\rho_\infty \epsilon_{ijk} \Omega_j G_k - \rho_\infty g \tag{6}$$

The pressure $\bar{p}$ in (5) is thus the deviation from $\bar{P}$ defined by (6). We have adopted the meteorological convention of using $(x, y, z) = (x_1, x_2, x_3)$ as the axes in the streamwise, spanwise, and wall-normal directions, respectively. The nondimensional temperature, θ, is defined as

$$\theta = \frac{T - T_\infty}{T_\infty} \tag{7}$$

where T and T_∞ are the local and reference temperatures, and $< ... >$ denotes averaging over (x, y) planes. In large-scale meteorological applications, the 'potential' temperature is used to distinguish between adiabatic and diabatic temperature change. At the scales considered in this idealization, the hydrostatic pressure variation across the depth of layer is small, and there is a negligible difference between the actual temperature and 'potential' temperature.

The SGS terms τ_S and q_S in (3) and (5) are defined as

$$\tau_{S,ij} = \overline{u_i u_j} - \bar{u}_i \bar{u}_j \qquad q_{S,j} = \overline{u_j \theta} - \bar{u}_j \bar{\theta} \tag{8}$$

and will be modelled. The models are the principal issue of this paper and are discussed below. The boundary conditions used are

$$\bar{u}_i = 0 \quad at \quad z = 0 \tag{9.1}$$

$$\bar{u}_i \rightarrow G_i \quad as \quad z \rightarrow \infty \tag{9.2}$$

$$\bar{\theta} = \bar{\theta}_0 \quad at \quad z = 0 \tag{9.3}$$

$$\bar{\theta} \rightarrow 0 \quad as \quad z \rightarrow \infty \tag{9.4}$$

4

All dependent variables are assumed to be periodic in the planes of homogeneity (x, y).

The solution technique employed is fully spectral in all three Cartesian dimensions and second order accurate in time. The explanation of the method requires some length, and the reader is referred to Coleman, *et al.*[5] for a complete discussion. In short, the semi-infinite domain $0 \leq z \leq \infty$ is mapped into a finite domain $1 \geq \eta \geq 0$ *via* the transformation $\eta = e^{-z/Z}$, where Z is a mapping length scale. Fourier methods are used to represent variables in the homogeneous (x, y) directions. A family of orthogonal Jacobi polynomials is used to generate basis functions in the variable η. Therefore, each dependent variable is a generalized Fourier series; for example,

$$u(x, y, \eta) = \sum_{k_x} \sum_{k_y} \sum_{m=0}^{M} \alpha_m(k_x, k_y) H_m(\eta) e^{i(k_x x + k_y y)} \qquad (12)$$

where each H_m is a basis function unique to u that satisfies the boundary conditions. The basis functions used for u, v, and w satisfy the continuity equation (4) everywhere so a Poission solution for pressure is not required.

In Fourier space, a filter may be defined by a wavenumber 'cutoff'; that is, wavenumbers higher than some value k_c are discarded and a finite series is formed. The cutoff filter has a length scale defined as $\overline{\Delta} = \pi/|k_c|$, and it can easily be shown that this filter commutes with differentiation. For variables represented by polynomial basis functions, the use of a finite series implies an effective 'cutoff' filter that, in general, *does not* commute with differentiation. In this study, a filter is defined explicitly as follows

$$\overline{u}(x, y, \eta) = \sum_{k_x} \sum_{k_y} \sum_{m=0}^{M} f_m \alpha_m(k_x, k_y) H_m(\eta) e^{i(k_x x + k_y y)} \qquad f_m = e^{-\gamma m^2} \qquad (13)$$

where γ is a constant. We make the assumption that this filter commutes with η differentiation (or equivalently, with z differentiation); this is justified by two observations. First, the α_m coefficients decay rapidly at high m. Since any error in a 'cutoff' series is directly related to the magnitude of the first few eliminated coefficients, this error will be small. Second, the additional application of the explicit filtering factor f_m reduces the importance

5

of these coefficients even further; in the specific cases presented in this paper, $\gamma \approx 0.01$, which results in the last coefficient of a typical series (i.e. $M = 20$) being multiplied by $f_m \approx 0.02$.

At first, it may seem simpler to apply an m 'cutoff' filter to the above series rather than use the f_m approach. However, the continuity equation puts constraints on the relationships among the α_m coefficients; a large, computationally expensive linear set of equations must be solved if M is to be reduced and the boundary conditions satisfied. Application of the filtering factor f_m retains both the continuity constraint and boundary conditions, and is computationally efficient.

The definition of this explicit filter in the *inhomogeneous*, or z direction, allows one to examine its effect on dynamic subgrid scale model. This will be discussed in detail in the next section.

LES Modelling

The SGS terms defined in (8) are modelled as follows

$$\tau_{S,ij} - \frac{\delta_{ij}}{3}\tau_{S,kk} = -2\nu_T \overline{S}_{ij} \qquad \nu_T = C\overline{\Delta}^2 |\overline{S}|\overline{S}_{ij} \tag{14.1}$$

$$q_{S,j} = -\frac{\nu_T}{Pr_T}\frac{\partial\overline{\theta}}{\partial x_j} = -\kappa_T\frac{\partial\overline{\theta}}{\partial x_j} \tag{14.2}$$

The composite length scale $\overline{\Delta}$ is defined as $(\overline{\Delta}_x\overline{\Delta}_y\overline{\Delta}_z)^{1/3}$. The coefficient C and turbulent Prandtl number Pr_T are computed by the dynamic procedure proposed by Germano *et al.*. In this procedure a test filter (denoted by a tilde, i.e. $\widetilde{\overline{u}}$) with length scale $\widetilde{\overline{\Delta}} > \overline{\Delta}$ is applied to the LES flow field. The resolvable stress and heat flux terms are computed from

$$L_{ij} = \widetilde{\overline{u}_i\overline{u}_j} - \widetilde{\overline{u}}_i\widetilde{\overline{u}}_j \tag{15.1}$$

$$K_j = \widetilde{\overline{u}_j\overline{\theta}} - \widetilde{\overline{u}}_j\widetilde{\overline{\theta}} \tag{15.2}$$

L_{ij} and K_j can then be expressed in terms of modelled quantities

$$L_{ij} = -2C(\widetilde{\overline{\Delta}}^2|\widetilde{\overline{S}}|\widetilde{\overline{S}}_{ij} - \overline{\Delta}^2\widetilde{|\overline{S}|\overline{S}}_{ij}) = -2CM_{ij} \tag{16.1}$$

6

$$K_j = -\frac{C}{Pr_T}(\widetilde{\overline{\Delta}^2}|\widetilde{\overline{S}}|\widetilde{\frac{\partial \overline{\overline{\theta}}}{\partial x_j}} - \overline{\Delta}^2|\overline{S}|\widetilde{\frac{\partial \overline{\theta}}{\partial x_j}}) = -\frac{C}{Pr_T}N_j \qquad (16.2)$$

Values of C and Pr_T can be determined by contracting both sides of (16.1) and (16.2) with M_{ij} and N_j, respectively, in a least squares approach suggested by Lilly[6].

We have not yet defined the test filter or the spatial dependence of C and Pr_T. To address this issue, we note that past researchers who used the dynamic model in flows with an inhomogeneous direction, e.g. the wall normal direction in turbulent channel flow, have not test filtered in this direction[3,4]. We shall call this form of test filtering 2D *filtering*. A typical test filter length scale of twice the 'regular' LES filter length in each homogenous direction, or

$$\widetilde{\overline{\Delta}}_x = 2\overline{\Delta}_x, \qquad \widetilde{\overline{\Delta}}_y = 2\overline{\Delta}_y, \qquad and \qquad \widetilde{\overline{\Delta}}_z = \overline{\Delta}_z \qquad (17)$$

was used. In the preceding section, we defined an explicit filter in the inhomogeneous direction. This enables us to test filter in all three dimensions, with $\widetilde{\overline{\Delta}}_z \approx 2\overline{\Delta}_z$ at all z points. The length scales $\widetilde{\overline{\Delta}}_z$ and $\overline{\Delta}_z$ are computed numerically by measuring the width of a filtered delta function $\delta(z - z_k)$ for both the regular and test filters. The composite length scale ratio $\widetilde{\overline{\Delta}}/\overline{\Delta}$ generally varies between 1.85 and 2.15 in a typical application. We shall call this form of test filtering 3D *filtering*.

To address the issue of C and Pr_T spatial dependence, we adopt the procedure of Germano *et al.*, and plane average the tensorial quantities in (16.1) and (16.2) before solving

$$C = -\frac{1}{2}\frac{<L_{ij}M_{ij}>}{<M_{ij}M_{ij}>} \qquad (18.1)$$

$$Pr_T = -C\frac{<N_jN_j>}{<K_jN_j>} \qquad (18.2)$$

This averaging procedure is necessary to remove local instabilities that result from pointwise calculations of C. The spatial dependence of ν_T and Pr_T is therefore restricted to the normal directions

$$\nu_T(z) = C(z) \cdot \overline{\Delta}^2 < |\overline{S}| > \qquad (19.1)$$

$$\kappa_T(z) = \nu_T(z)/Pr_T(z) \qquad (19.2)$$

7

with both quantities also being functions of time. This procedure is used for both $2D$ and $3D$ filtering.

The spatial dependence of C and Pr_T is the subject of ongoing research. Ideally, C and Pr_T could be functions of (x,y,z,t); the procedure of plane averaging to remove (x,y) dependence has been found to produce acceptable results. This is an area needing considerable attention for flows which are not homogeneous in these planes. Local averaging techniques in both space and time are currently under investigation to remove this restriction[7].

LES of the Neutral Ekman Layer

The dynamic model was applied to LES of a neutral Ekman layer to examine the differences between $2D$ and $3D$ filtering. The neutral Ekman layer is that defined by solving $(3),(4)$ with gravity $g = 0$. The case considered here is defined by the following parameters

$$Re = \frac{|\mathbf{G}|D}{\nu}, \qquad D = (\nu/|\Omega|)^{1/2}, \qquad \mathbf{G} = (G_x,0,0), \qquad \Omega = (0,0,\Omega_z) \qquad (20)$$

Coleman performed a direct numerical simulation (DNS) for $Re = 500$ using a 128x128x50 grid with length 2δ in each of the (x,y,z) directions, where δ is the boundary layer thickness. In this study, two LES grids with the same lengths as the DNS grid were used, a coarse 32x32x21 grid and a fine 32x32x30 grid. The runs are labeled with a grid resolution prefix and test filtering suffix, e.g. *Coarse2D*. Flow statistics are generated by time averaging until the mean profiles satisfy the Reynolds-averaged momentum equations to within two percent of the equilibrium value. All results presented in this section are time-averaged.

The friction velocity, u_*, and surface shear stress angle, β, are the primary global quantities used for comparisons. Table I gives the values of u_*, β, and the amount of resolved turbulent kinetic energy (TKE) for all LES runs, along with the results from Coleman's DNS (since u_* and β are derived from mean quantities, filtering the DNS results will have a negligible effect on these values). The results show that $3D$ filtering significantly improves the coarse grid calculation. Indeed, the results from the *Coarse3D* calculation are better than those from the *Fine2D* calculation. The accuracy of the LES

8

correlates well with the fraction of TKE that is resolved, and in all cases the SGS terms are required to model a significant portion of the flow field.

The eddy viscosity $\nu_T(z)$ is shown in Figure 1a for both the near wall and far field regions. The most striking difference is the large disparity in ν_T between $3D$ and $2D$ filtering runs in the outer regions of the flow, with significant deviation first occurring around $z^+ = 30$. Large values of ν_T reduce the TKE, leading to a less turbulent flow as measured by u_* and β (laminar Ekman layers have $\beta = 45^o$, while an 'infinitely turbulent' Ekman layer would have $\beta \to 0^o$).

Varying the grid resolution affects the profile of ν_T. In Figure 1b, the coefficient $C(z)$ in (19.1) is shown. In the near wall region $0 \leq z^+ \leq 30$, $C(z)$ is essentially independent of grid resolution *and* the filtering technique. This produces lower ν_T for the *Fine2D* and *Fine3D* runs in the near wall region, since the value of $\overline{\Delta}^2$ is smaller on the fine grid than the coarse grid. In the outer region, however, the *Fine2D* ν_T is nearly the same as that of *Coarse2D*, so that in *Fine2D* and *Coarse2D* the same amount of SGS energy is modelled. The same behavior is observed in *Fine3D* and *Coarse3D*. This indicates that the extra resolution in the outer region for fine grid calculations does not provide any benefit, and that the accuracy of the calculation in the outer region cannot be improved unless a finer grid in the streamwise and spanwise directions is introduced. Note that the values of $C(z)$ for *Fine2D* and *Fine3D* are larger than their coarse grid counterparts in the outer region.

From Table I we note that while the *Fine3D* case is the most accurate, it does not represent a substantial improvement over *Coarse3D*. We can infer this from Figure 1a, since the *Coarse3D* and *Fine3D* values of ν_T are very close in the entire flow, except for the near wall region.

LES of the Stratified Ekman Layer

In this section, we shall examine the behavior of the dynamic subgrid scale model when a mean temperature profile is imposed upon the Ekman layer. The equations governing the flow are $(3) - (5)$, with the gravity force g nonzero.

The temperature profile will be suddenly imposed on the *Fine2D* and *Fine3D* neutral cases of the preceding section at time $t_i = 0$. The profile is the symmetric error-function

9

used by Coleman as an idealization of the Convective Boundary Layer (CBL), and is shown in Figure 2. The profile has both an unstable region, caused by a surface heat flux, and a stable region, due to a capping inversion some distance above the surface. An initial surface lapse rate $\Gamma_{0,i}$ is selected and incorporated into a surface Richardson number

$$Ri_{0,i} = \frac{g\Gamma_{0,i}D^2}{T_\infty|\mathbf{G}|^2} \tag{21}$$

where 0 subscripts denote surface values. The values of the shape factors and surface Richardson number were selected as $a_* = 4D$, $b_* = 5D \approx 0.4\delta$, and $Ri_{0,i} = -0.05$ to produce flow conditions consistent with the 'moderate heating' DNS case of Coleman. Unfortunately, direct comparison between DNS and LES is not possible for the stratified flow cases due to a slight difference in Reynolds numbers. However, correct interpretation of the LES data should be possible considering the well known 'mixed-layer' behavior of the CBL[2]. In addition to the two LES involving the dynamic model, a third case, denoted *Constant*, was run with constant values of the Smagorinsky coefficient $C = 0.008$ and $Pr_T = 0.5$ to illustrate the shortcomings of such an approach in the stratified Ekman layer. The definition of C and the calculation of length scales is somewhat different between our LES and 'standard' finite-difference techniques employed by the meteorological community[2]; our C corresponds to a Smagorinsky constant $C_s \approx 0.2$.

Figure 3 shows the time histories of global TKE for the *Fine2D*, *Fine3D*, and *Constant* cases with imposed temperature profiles. Time is normalized by the global rotation time scale, $f^{-1} = (2\Omega_z)^{-1}$. We shall refer to the first two cases as $H2D$ and $H3D$, respectively, since grid resolution is not varied. All cases display an initial transient of duration $tf \approx 0.4$. $H3D$ and $H2D$ then approach a state of quasi-equilibrium, while *Constant* displays a monotonic decrease in TKE. Quasi-equilibrium is a well known characteristic of the CBL[2,5] and is indicative of the rapid response of the turbulence on the time scale required to alter the mean θ profile. $H3D$ resolves more TKE than $H2D$, a characteristic observed in the neutral Ekman layer and attributed to a smaller value of $\nu_T(z)$. Time averaging is done for the period $1.5 \leq tf \leq 2.0$ to generate statistics; the slight unsteadiness in the flow field, along with the small sample time, produces some statistical uncertainty. Unless otherwise noted, the quantities for $H3D$ and $H2D$ are assumed time-averaged over this interval.

10

Time averaging is not done for *Constant*, due to the absence of a quasi-equilibrium state; instead, instantaneous profiles at $tf = 1.62$ are used.

Figure 4 shows the mean θ profile along with the initial temperature profile. Both $H3D$ and $H2D$ are close, and both deviate substantially from *Constant*. The tendency of the Smagorinsky model to smear the capping inversion was first observed by Deardorff[8], and is also observed here. Figure 5 shows the buoyant heat flux $< w'\theta' >$ the minimum of which defines z_I, the inversion height and a relevant length scale for the CBL. $H3D$ and $H2D$ agree on the height of both z_I and the location of maximum heat flux. The profiles of θ and $< w'\theta' >$ agree closely with accepted behavior of the CBL, and demonstrate that within and above the stable inversion layer turbulent activity is largely suppressed. Coleman calculated the convection velocity, first used by Deardorff, as

$$w_* = (gQ_0 z_I/T_\infty)^{1/3} \qquad (22)$$

and showed that, when scaled with w_* and z_I, his DNS results are in excellent agreement with high-Re LES, laboratory, and field data. We will not repeat that exercise here; instead, a comparison of global quantities for similarly heated cases is shown in Table II. Good quantitative agreement between DNS and LES is observed. The quantity gz_I/T_∞ is essentially constant in both the DNS and LES; u_* does not vary much with Re, so we would expect u_*/w_* to be lower for the LES since the heating is slightly stronger. From the calculation of w_*, we note that the time averaging period for the LES statistics corresponds to roughly 2 'eddy turnover' times as defined by z_I/w_*.

Figures 6a and 6b show $\nu_T(z)$ and $C(z)$ near the wall and over the bulk of the CBL. There is a substantial difference between the $H2D$ and $H3D$ cases, with the 3D filtering procedure producing much lower values of ν_T and C, as was the case in the neutral layer. The values of ν_T diverge much closer to the wall than in the neutral case, with significant differences occurring at about $z^+ = 10$.

Figures 7a and 7b show profiles of $\kappa_T(z)$ and the turbulent SGS Prandtl number, defined as $Pr_T = \nu_T/\kappa_T$. Absolute values of Pr_T greater than three are observed in both $H3D$ and $H2D$ but are not shown; these large values occur when $\kappa_T \approx 0$. For $H2D$, Pr_T attains very large values at points within the CBL due the small values of κ_T. For $H3D$, Pr_T is close to unity for much of the region $0 \leq z/z_I \leq 0.5$, after which it drops to $Pr_T = 0.5$ in

11

the upper CBL, and then increases to $Pr_T \approx 2.5$ in the inversion above $z = z_I$. Most LES researchers use Pr_T values between 0.33 and 0.5 for the CBL[2]. One explanation for the behavior of Pr_T in this study is that at low Re, a significant portion of the CBL near the surface is still influenced by the surface shear, and shear layers require Pr_T close to 1.0. Only away from the surface, where the motion produced by buoyant eddies dominates, should Pr_T drop. In any case, it is important to note the variation of Pr_T with space and filtering technique (though we assume the $H2D$ results to be somewhat erroneous, as will be discussed later). Large variations of Pr_T with flow type, initial conditions, and even grid resolution have been reported by Moin *et al.*[4], and cast doubt on the practice of assuming constant Pr_T.

To the author's knowledge, the dynamic subgrid scale model is the first to permit accurate LES of neutral, stably stratified, and unstably stratified regimes of Ekman layer flow without the need for modifications like (e) and (f) presented in the introduction.

Discussion

I. Effects of Inhomogeneous Filtering on the Dynamic Model

As we witnessed in both neutral and stratified Ekman layer flow, there are marked differences in the subgrid scale stress and heat flux depending on whether $2D$ or $3D$ filtering is used in the dynamic calculation. A suspected criterion for this is as follows. When the velocity variance in the inhomogeneous direction, w', contributes significantly to the TKE, $3D$ filtering should be employed. This is seen in Figure 8a, which plots the three components of velocity variance in the neutral Ekman layer LES *Fine3D*. In the outer region, $u' \approx v' \approx w'$ and the turbulence is nearly isotropic. In this one region the largest difference between $2D$ and $3D$ filtering is observed.

If LES were done on a homogeneous, isotropic flow with equispaced grid points in all directions, it would be difficult to defend the practice of abandoning test filtering in one arbitrary direction while retaining it in the other two. Although the Ekman layer has an inner region which is quite inhomogeneous, its outer region, as well as outer regions of other external boundary layers, is nearly homogeneous and isotropic so $3D$ filtering should be required.

12

The $H3D$ and $H2D$ cases show a disparity in $\nu_T(z)$ much closer to the surface. This is expected, since surface heating produces a well mixed, relatively homogeneous flow with values of w_* that can exceed u_*. Figure 8b shows velocity variances for $H3D$. In the neutral layer, at $z^+ = 30$ a large disparity in $C(z)$ was observed; comparing magnitudes of velocity variances for $Fine3D$ and $H3D$ show that in $H3D$, the magnitudes are much closer at $z^+ = 30$ than in $Fine3D$. We would therefore expect a disparity to occur below this point for $H3D$.

The $H3D$ calculation of the CBL is significantly more accurate than the $H2D$ simulation, demonstrating that 2D filtering should be discouraged for the CBL. Indeed, many studies of the CBL using LES employ equispaced grids in all three directions to take advantage of the 'quasi-homogeneous' behavior. In such simulations, it should be an easy matter to test filter in all three dimensions.

A logical question is 'Why has the dynamic model had such success in turbulent channel flow without 3D filtering?' One possible explanation is that channel flow is internal; that is, it has a statistically steady state in which the pressure gradient balances the total shear stress gradient (sum of resolved and modelled components). The guarantee of a correct shear stress profile may make up for inadequacies present in the SGS modelling technique[9]. In an external boundary layer this is not possible.

II. Effects of Buoyant Forcing on the Dynamic Model

A single subgrid model applicable to neutral, unstable, and stable regimes of turbulent flow has been previously unrealized. As mentioned in the first section, several researchers proposed methods of alleviating the problem, which may be characterized as a need for the eddy viscosity to vary as the stratification changes.

The dynamic model shows the ability to extinguish the eddy viscosity in regions of strong stable stratification without resorting to *ad hoc* modifications. Also unnecessary is the additional expense of a SGS TKE equation to reduce the eddy viscosity in regions of damped turbulent activity (the solution of such an equation involves further terms that need to be parameterized). The dynamic calculation of ν_T and κ_T produces Pr_T values that are in good agreement with accepted values in the shear and convectively dominated

13

regions of the CBL. The failure of the Smagorinsky model with a constant C is evident in Figures 4 and 5. In addition to smearing the inversion layer, Figure 4 illustrates how the surface flux has been eradicated. This produces a poor heat flux profile that is inconsistent with well-known 'mixed-layer' behavior of the CBL. Conceivably, some of these deficiencies could be alleviated with the introduction of commonly used damping factors near the wall. In the spirit of model comparison, however, we have avoided *ad hoc* formulations.

The widespread success of the dynamic model is unparalled and leads one to believe that the model can be used for other scalar quantities. A specific scalar of interest is moisture, with the associated effects of condensation and evaporation. The introduction of such a scalar into the stratified Ekman layer idealization of the Planetary Boundary Layer will be the focus of future work.

Acknowledgments

References

[1] J. Smagorinsky, "General Circulation Experiments with the Primitive Equations. I. The Basic Experiment", Mon. Weather Review, 91, 99 (1963).

[2] F. M. Nieuwstadt, P. J. Mason, C. H. Moeng, and U. Schumann, "Large-Eddy Simulation of the Convective Boundary Layer: A Comparison of Four Computer Codes", 8th Symp. on Turbulent Shear Flows, Munich, Germany (1991).

[3] M. Germano, U. Piomelli, P. Moin, and W. Cabot, "A Dynamic Subgrid-Scale Eddy Viscosity Model", Center for Turbulence Research, Proceedings of the Summer Program, Stanford University and NASA/Ames Research Center (1990).

[4] P. Moin, K. Squires, W. Cabot, and S. Lee, "A Dynamic Subgrid-Scale Model for Compressible Turbulence and Scalar Transport", Phys. Fluids A, 3, 2746 (1991).

[5] G. Coleman, J. Ferziger, and P. Spalart, "A Numerical Simulation of the Stratified Turbulent Ekman Layer", Dept. of Mech. Eng., Stanford University, Thermosciences Division Report TF-48 (1990).

[6] D. Lilly, Private Communication (1991).

[7] U. Piomelli, J. Ferziger, and P. Moin, "Models for Large Eddy Simulation of Turbulent Channel Flows Including Transpiration", Dept. of Mech. Eng., Stanford University, Thermosciences Division Report TF-32 (1987).

[8] J. W. Deardorff, "The use of Subgrid Transport Equations in a Three-Dimensional Model of Atmospheric Turbulence", J. Fluids Eng., **95**, 429 (1973).

[9] U. Piomelli, Presentation at the 44th Annual Meeting of the American Physical Society, Division of Fluid Dynamics, Scottsdale, Arizona (1991).

TABLE I

Global Results for Neutral Ekman Layer with Re = 500

Grid and Filter	$u_* \times 10^2$	β (deg)	Resolved TKE (DNS = 1)
128x128x50			
DNS	6.27	25.4	1.0
32x32x21			
Coarse 2D	5.83	29.7	0.49
Coarse 3D	6.00	27.3	0.64
32x32x30			
Fine 2D	5.93	28.9	0.58
Fine 3D	6.02	27.3	0.70

TABLE II

Global Results for Stratified Ekman Layer

Grid	$Ri_{0,i}$	tf	$u_* \times 10^2$	β (deg)	u_*/w_*
128x128x50					
DNS	-0.04	2.1	7.48	28.1	0.93
32x32x30					
$H3D$	-0.05	$1.5 - 2.0$	6.93	29.2	0.95
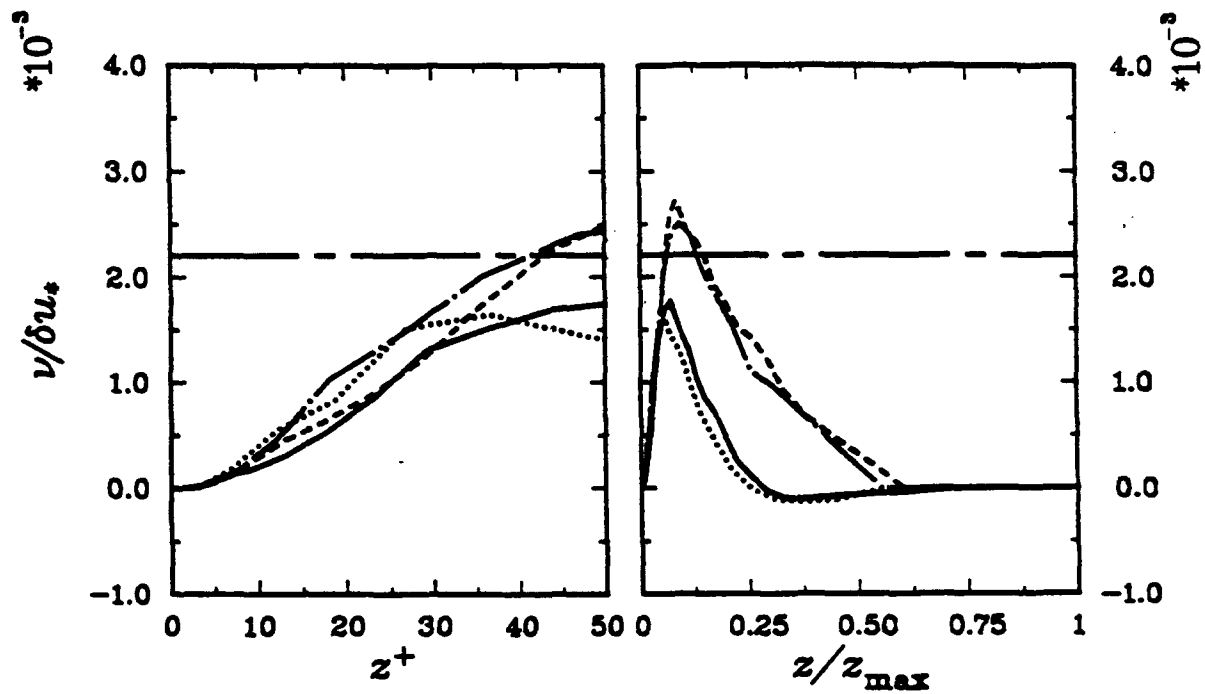
Figure 1a. Eddy viscosity for neutral Ekman layer. —— , *Fine3D*, ---- , *Fine2D*, ⋯⋯ , *Coarse3D*, —·— , *Coarse2D*
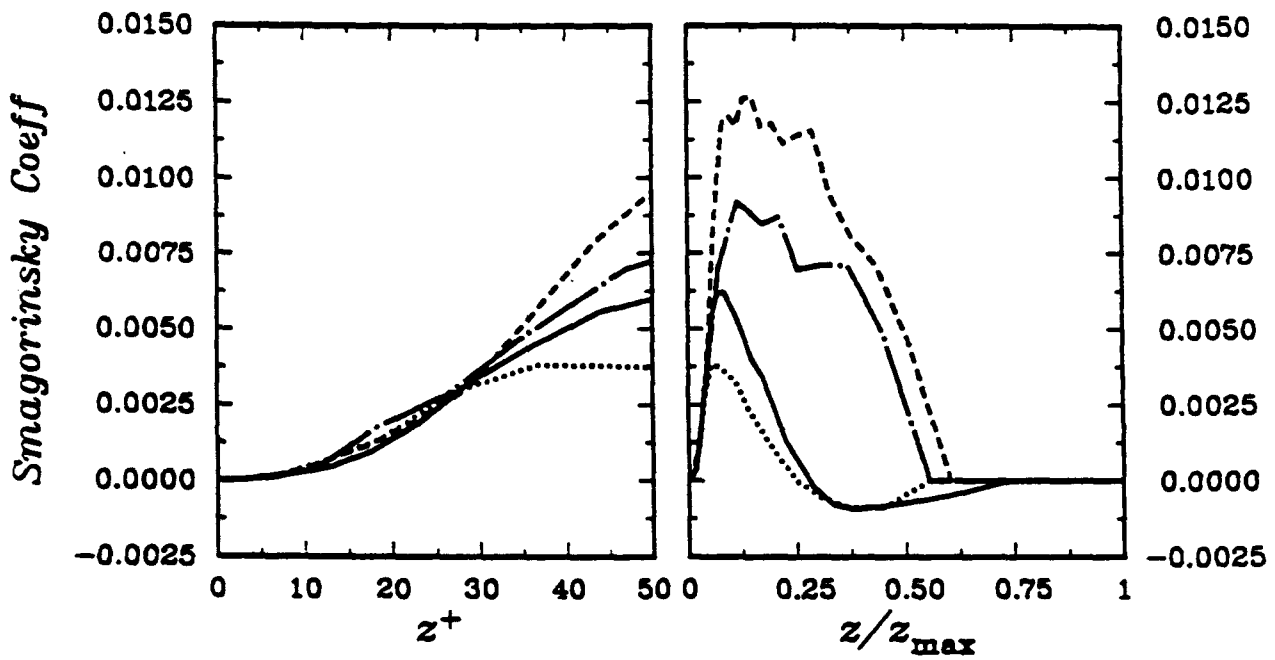
Figure 1b. Smagorinsky coefficient for neutral Ekman layer. —— , *Fine3D*, ---- , *Fine2D*, ········ , *Coarse3D*, —·— , *Coarse2D*
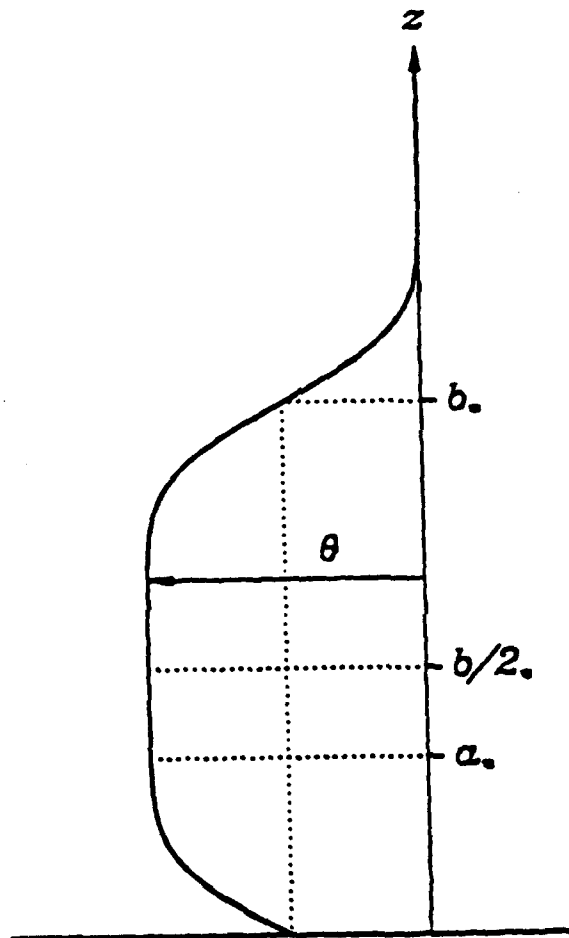
Figure 2. Initial temperature profile.
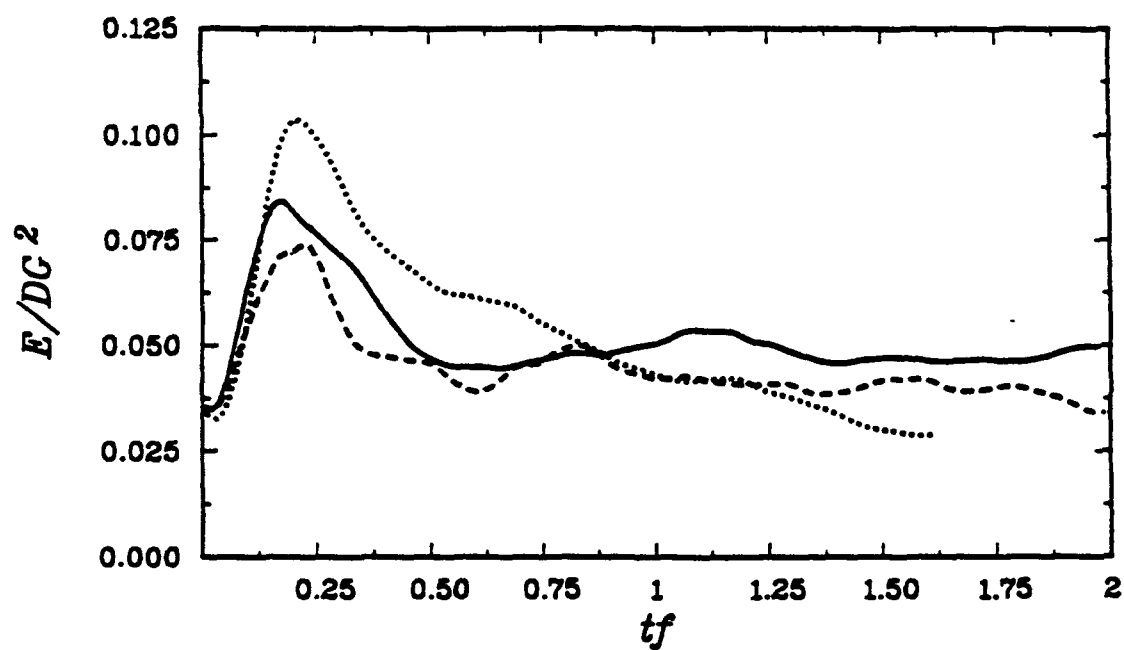
Figure 3. Time history of globally integrated TKE for stratified Ekman layer. ——— , $H3D$, ---- , $H2D$, ········ , $Constant$
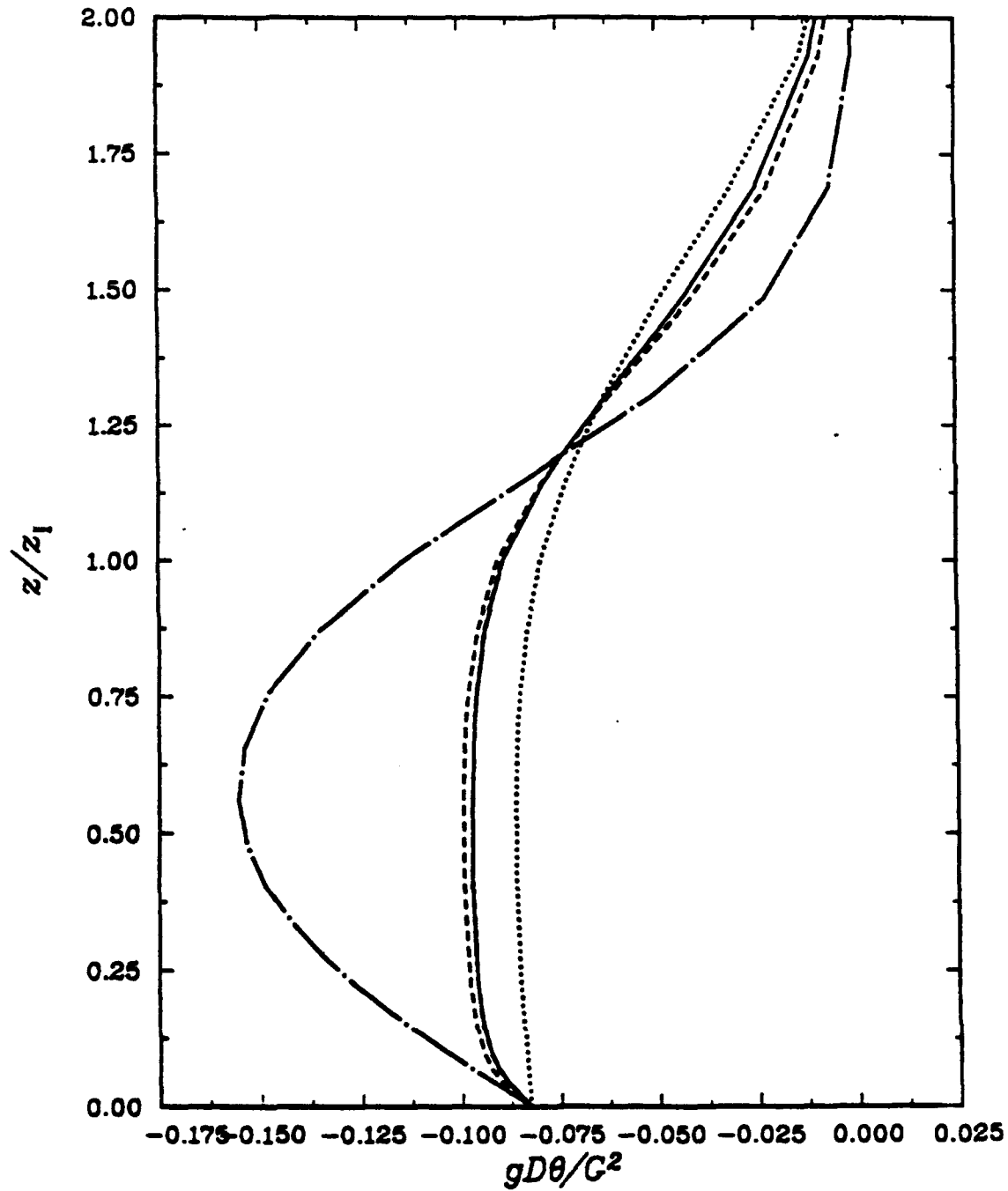
Figure 4. Mean Θ profiles for stratified Ekman layer. ——– , $H3D$, ---- , $H2D$, ········ , *Constant*, —·— , Initial condition.
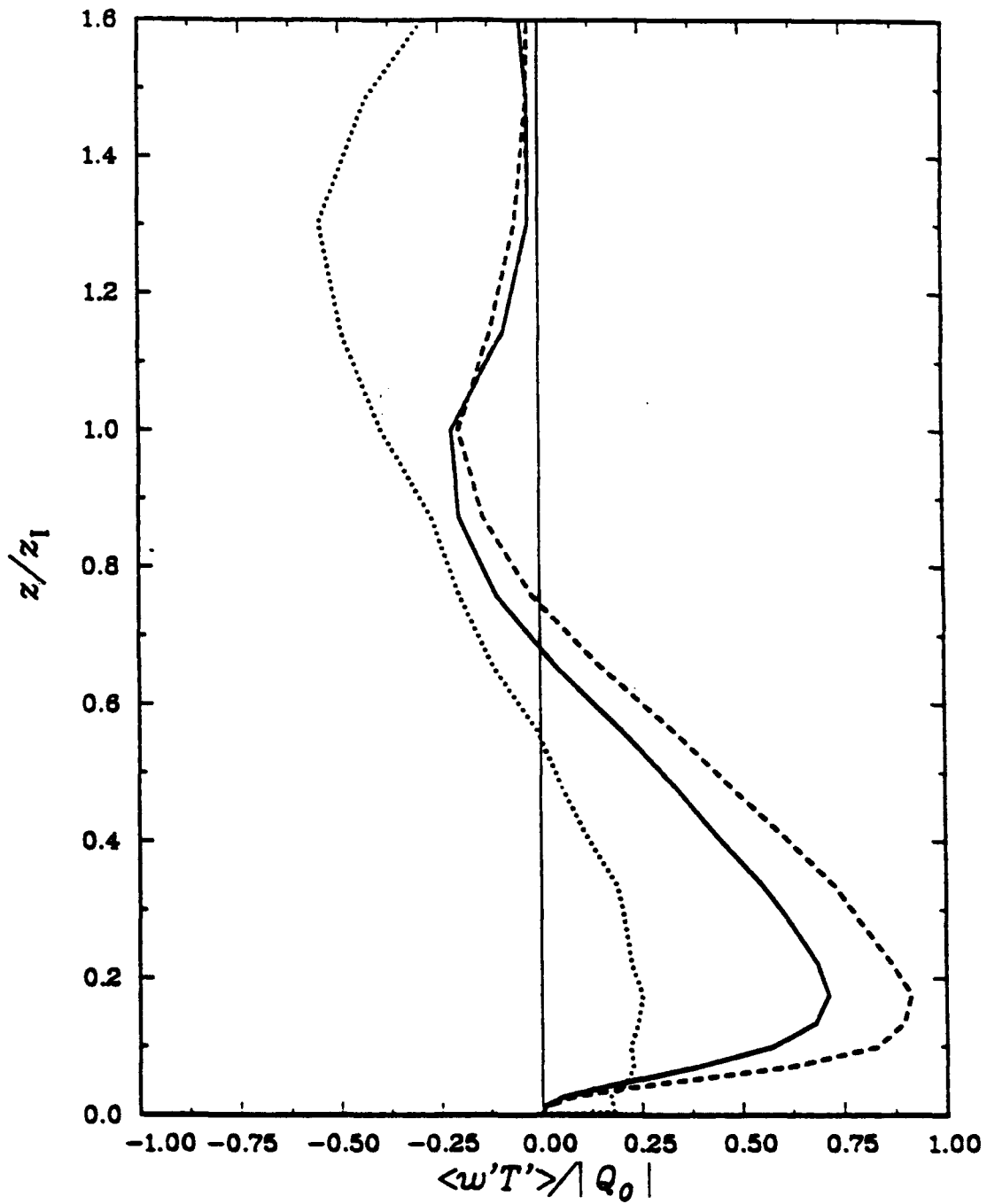
Figure 5. Mean heat flux for stratified Ekman layer (sum of resolved and modelled parts). ——— , $H3D$, - - - - , $H2D$, ········· , $Constant$.
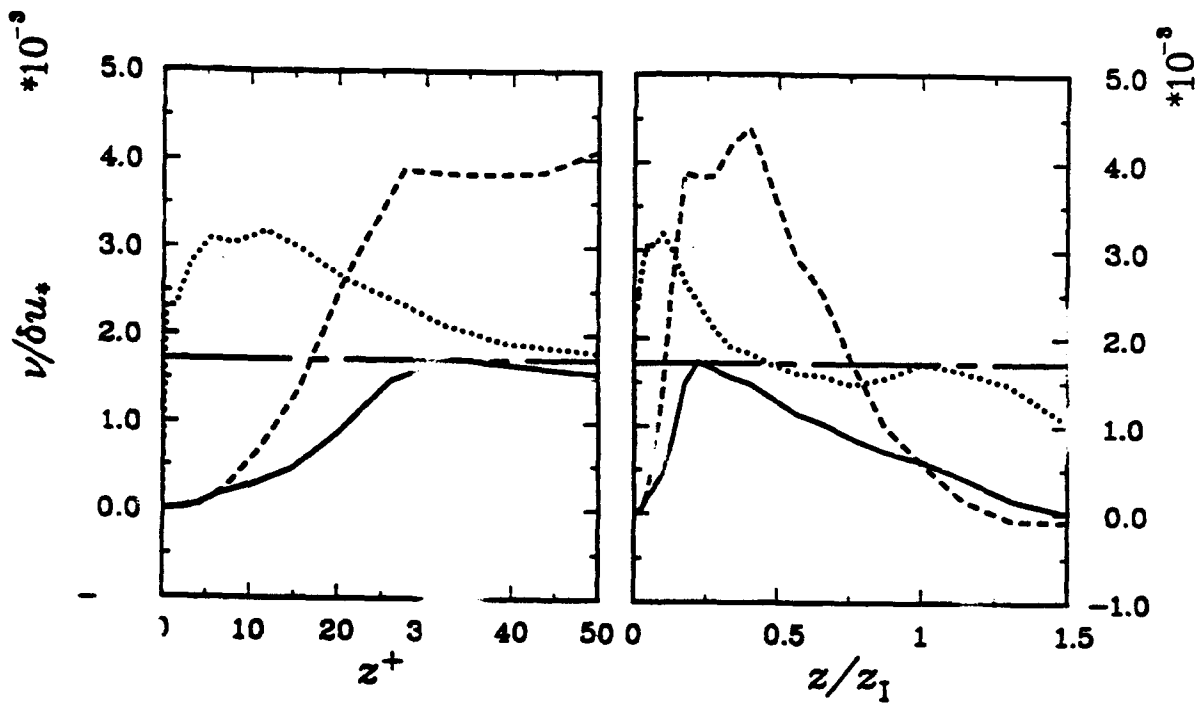
Figure 6. Eddy viscosity for stratified Ekman layer. —— , $H3D$, ---- , $H2D$, ⋯⋯ Constant, —·— , Molecular ν.
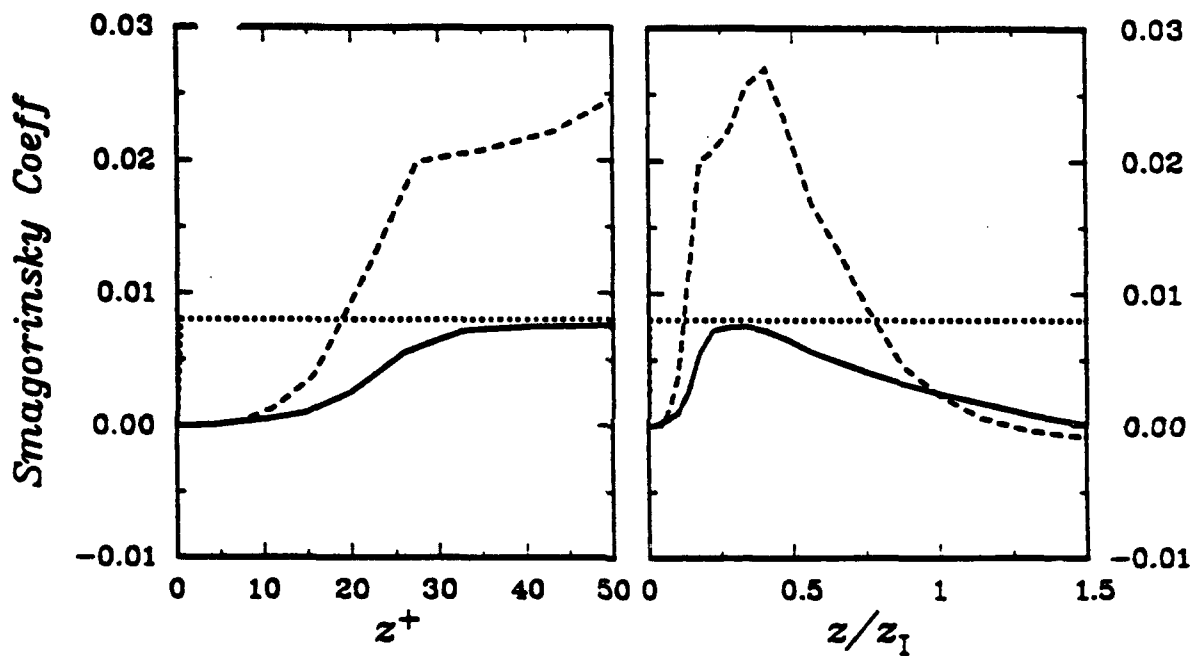
Figure 6b. Smagorinsky Coefficient for stratified Ekman layer. ——— , *H3D*, ---- , *H2D*, ········ , *Constant.*
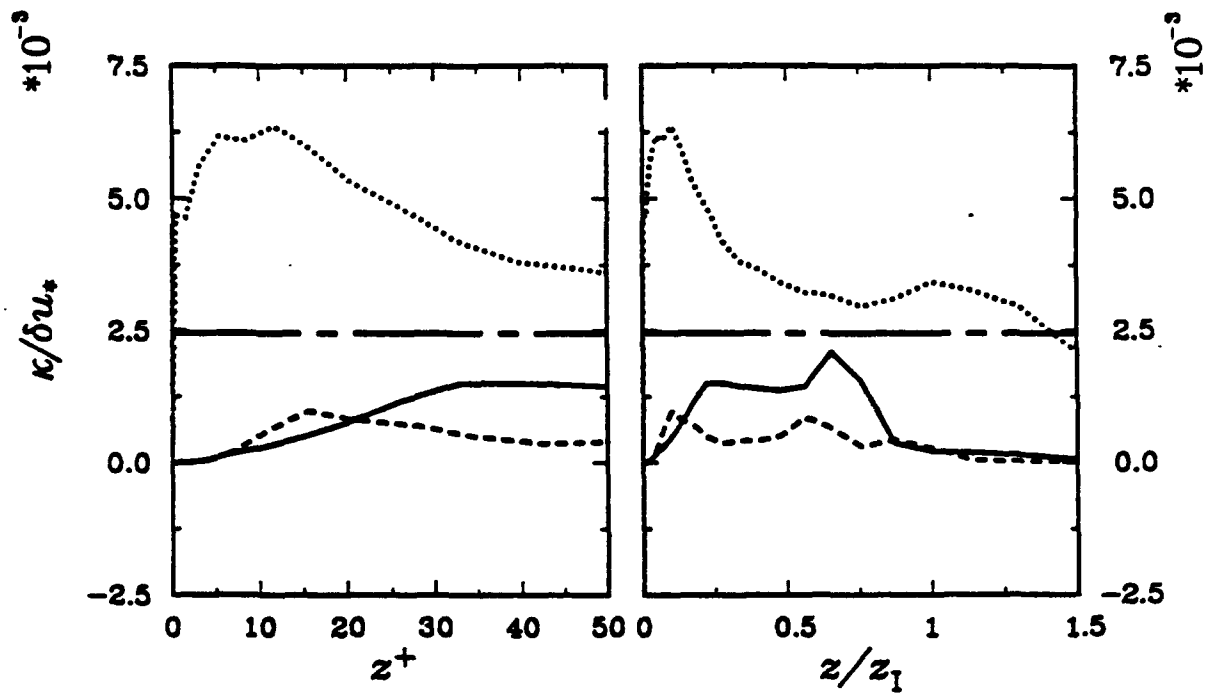
Figure 7a. Thermal diffusivity for stratified Ekman layer. —— , $H3D$, ---- , $H2D$, ········ , *Constant*, —·— , Molecular κ.
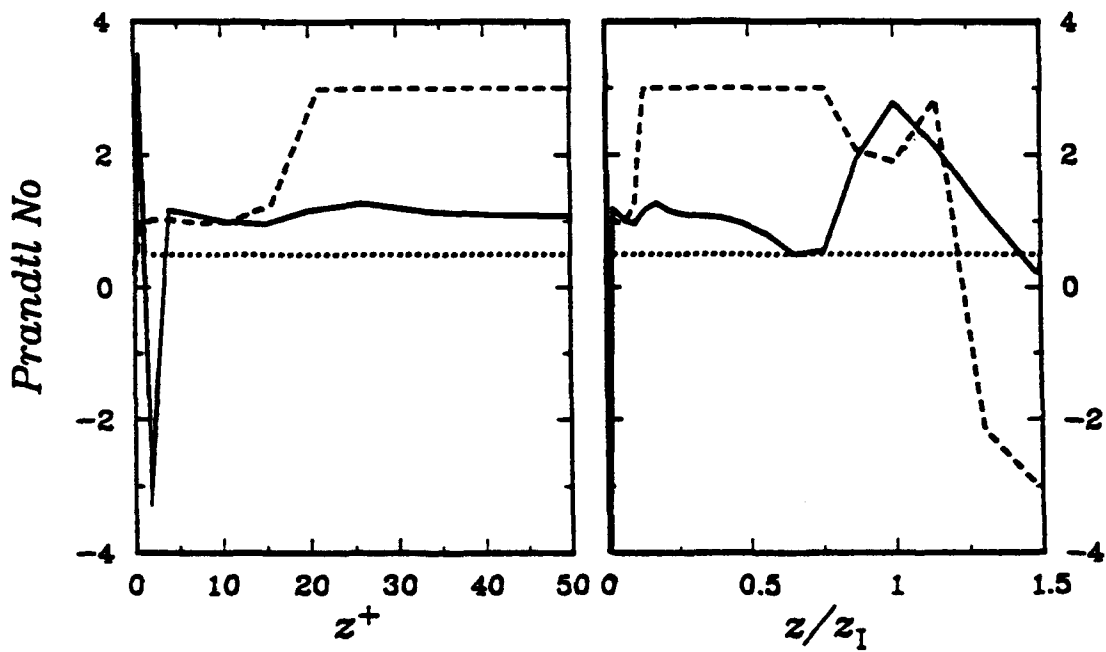
Figure 7b. Prandtl number for stratified Ekman layer, $|Pr_T| > 3$ not shown. ——— , $H3D$, - - - - , $H2D$, ········ , $Constant$.
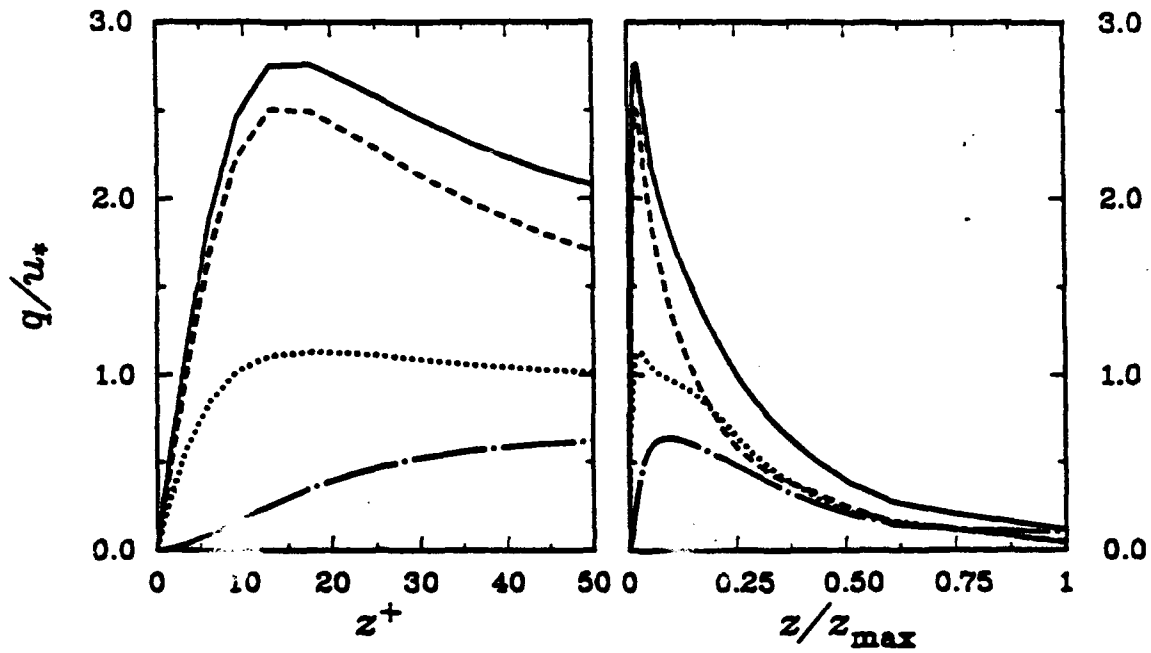
Figure 8a. Velocity variance for neutral Ekman layer case *Fine3D*. —— , total, ---- , u (streamwise), ········ , v (spanwise), —·— , w (vertical).
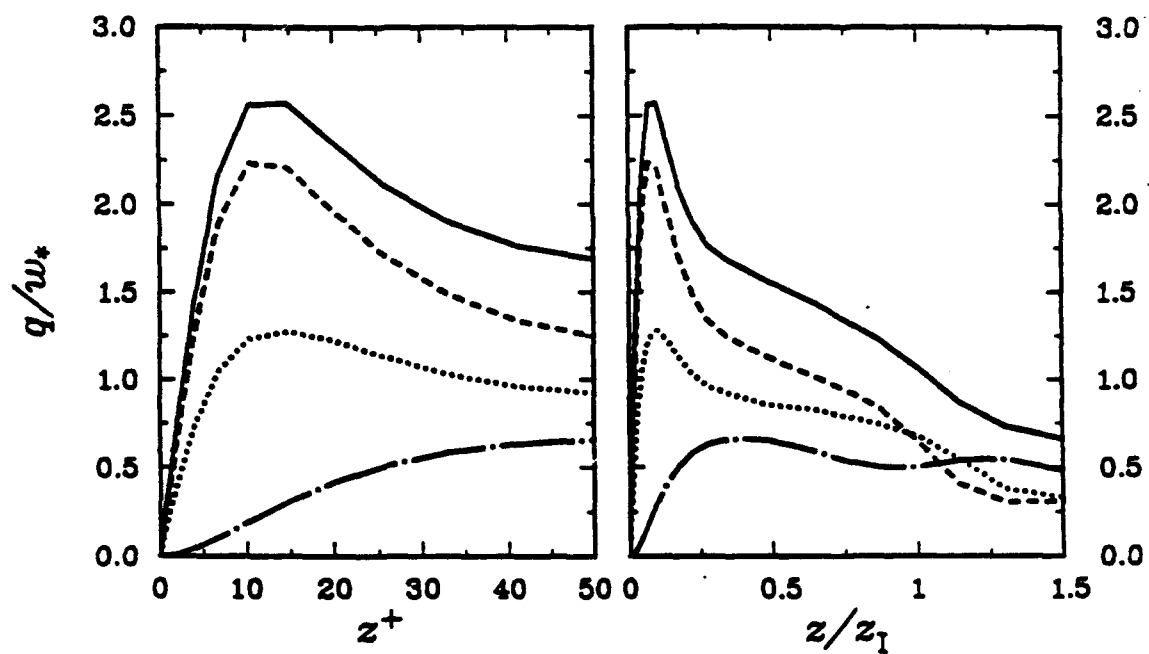
Figure 8b. Velocity variance for stratified Ekman layer case $H3D$. ———, total, ----, u (streamwise), ········ , v (spanwise), —·—, w (vertical).